Localization of Propagative Phonons in a Perfectly Crystalline Solid

S. Pailhès,[1,*] H. Euchner,[2,3] V. M. Giordano,[1,9] R. Debord,[1] A. Assy,[5] S. Gomès,[6] A. Bosak,[4] D. Machon,[1] S. Paschen,[7] and M. de Boissieu[8,9]

[1]*Institute of Light and Matter, UMR5306 Université Lyon 1-CNRS, Université de Lyon 69622 Villeurbanne cedex, France*
[2]*Institut für Theoretische und Angwandte Physik, Universität Stuttgart, D-70550 Stuttgart, Germany*
[3]*Institute of Materials Science and Technology, Vienna University of Technology, A-1040 Vienna, Austria*
[4]*European Synchrotron Radiation Facility, BP 220, F-38043 Grenoble cedex, France*
[5]*Université de Lyon, INSA-Lyon, CETHIL UMR5008, F-69621 Villeurbanne, France*
[6]*Université de Lyon, CNRS, CETHIL UMR5008, F-69621, France*
[7]*Institute of Solid State Physics, Vienna University of Technology, 1040 Vienna, Austria*
[8]*Université Grenoble Alpes, SIMAP, F-38000 Grenoble, France*
[9]*CNRS, SIMAP, F-38000 Grenoble, France*

(Received 28 February 2014; published 11 July 2014)

Perfectly crystalline solids are excellent heat conductors. Prominent counterexamples are intermetallic clathrates, guest-host systems with a high potential for thermoelectric applications due to their ultralow thermal conductivities. Our combined experimental and theoretical investigation of the lattice dynamics of a particularly simple binary representative, Ba_8Si_{46}, identifies the mechanism responsible for the reduction of lattice thermal conductivity intrinsic to the perfect crystal structure. Above a critical wave vector, the purely harmonic guest-host interaction leads to a drastic transfer of spectral weight to the guest atoms, corresponding to a localization of the propagative phonons.

DOI: 10.1103/PhysRevLett.113.025506 PACS numbers: 63.20.kg

Low thermal conductivity is usually associated with highly disordered, aperiodic, nanostructured, or even amorphous solids [1–3]. However, certain materials conduct heat poorly in spite of a perfectly crystalline structure. Understanding the mechanism of this phenomenon is not only of fundamental interest but also highly relevant for the field of thermoelectric energy conversion [4,5]. A thermoelectric material should combine low thermal conductivity with high electron mobility. A class of materials that has proven to perfectly meet the above requirement is intermetallic clathrates of which the type-I clathrate Ba_8Si_{46} is the simplest representative [6,7]. It is a guest-host system in which Ba fills large polyhedral cavities in a covalently bound, fully ordered Si framework [Fig. 1(b)]. Experimentally, coherent coupling of the guest atoms to the dynamics of the host lattice was evidenced [8,9]. However, no significant broadening of the acoustic phonon linewidth has been found, thus emphasizing that essentially no anharmonic scattering is present [9]. The main effect observed is an abrupt spectral weight transfer between acoustic and guest-optical phonons [9]. Similar effects of harmonic spectral weight changes are observed in other complex materials such as clathrate hydrates [10,11], skutterudites [12], or quasicrystals [1]. From *ab initio* studies it has been proposed that these effects are related to changes in the vibrational nature of propagative phonon modes when approaching the flat optical branches [9]. Localization and changes in the characteristics of propagative phonon modes are known to occur in amorphous materials [2], in quasicrystals [13], and in nanostructured materials [3]. In these materials, the vibrational nature of the excitations and therefore of the heat transport [2] is altered. In this context the key question we address in clathrates is as follows: are propagating phonons scattered by usual scattering mechanisms such as Umklapp scattering or is there rather a mechanism of mode localization leading to a change in the vibrational nature of acoustic harmonic phonons, which then results in a change of the energy transport mechanism? We provide a direct comparison between experimental and theoretical results of the lattice dynamics in the emblematic binary silicon clathrate Ba_8Si_{46}, using inelastic x-ray scattering and *ab initio* density functional theory (DFT) calculations. Due to the

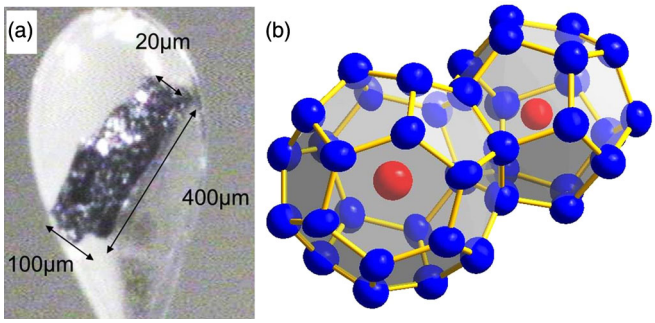

FIG. 1 (color online). (a) Ba_8Si_{46} microcrystal grown at 5 GPa and 1000°C. (b) Representation of face sharing $BaSi_{20}$ and $BaSi_{24}$ cages as building units of type-I clathrates. Atoms are represented by their atomic displacement ellipsoids obtained from single crystal x-ray diffraction.

absence of vacancies and transition metal atoms in the host framework of Ba_8Si_{46}, this binary clathrate offers the unique opportunity to investigate the intrinsic mechanism of the guest-host interaction. Experiment and DFT simulations show excellent agreement and clearly evidence spectral weight transfer from framework-dominated acoustic phonon modes to flat optical branches when reaching a critical wave vector. Then again, the absence of a broadening of the acoustic modes in the experimental data excludes usual scattering mechanisms as main cause of the reduced lattice thermal conductivity. This, together with changes in the vibrational nature of the acoustic phonon modes, as extracted from our simulations, points to a localization mechanism of propagative phonons being responsible for the reduction of lattice thermal conductivity in guest-host systems.

High-quality microcrystals of the binary clathrate Ba_8Si_{46} [Fig. 1(a)] were synthesized under extreme conditions (high pressure and high temperature). They show low thermal conductivity of about 1.7 W/mK at ambient temperature (see Supplemental Material [14]). The crystal structure was obtained from x-ray single crystal diffraction on a synchrotron source (see Supplemental Material [14]). The lattice dynamics was probed by inelastic x-ray scattering (IXS) at the ESRF beamline ID28. Longitudinal and transverse phonon modes, propagating along $[0,0,h]$ (LA_{001}) and $[h,h,0]$ (TA^{001}_{110}), respectively, were measured by constant $\mathbf{Q}$ scans around the $\mathbf{G} = (0,0,6)$ Bragg reflection [15]. Additional measurements, conducted for longitudinal phonons propagating along the $[h,h,0]$ and the $[h,h,h]$ directions are presented in the Supplemental Material [14]. In order to extract the intrinsic position, width, and intensity of a phonon, represented by the dynamical structure factor (DSF), from the measured scattering profiles, we apply an advanced fitting procedure, using damped harmonic oscillators for acoustic phonons and Gaussian functions for the low-lying optical excitations. The instrumental momentum resolution is $\Delta Q = 0.035$ Å^{-1}, while the energy resolution for dispersive modes is of the order of 2 meV. Detailed considerations on the IXS cross section, the experimental setup, the instrumental resolution, and the fitting procedure are discussed in the Supplemental Material [14]. The lattice dynamics of Ba_8Si_{46} was simulated by *ab initio* DFT calculations, using the DFT code VASP in combination with the PHONON package (see Supplemental Material [14]). The scattering function and the IXS differential cross section were determined from these calculations and provided initial conditions for the fitting procedure.

In Figs. 2(a) and 2(c) we present the experimentally determined energy positions of longitudinal (LA_{001}) and transverse (TA^{001}_{110}) phonons on top of the simulated IXS spectra shown as color mapping. In contrast to Ge-based clathrates [9], only a small rescaling of the energy axis of 1.07 is necessary to achieve excellent agreement between

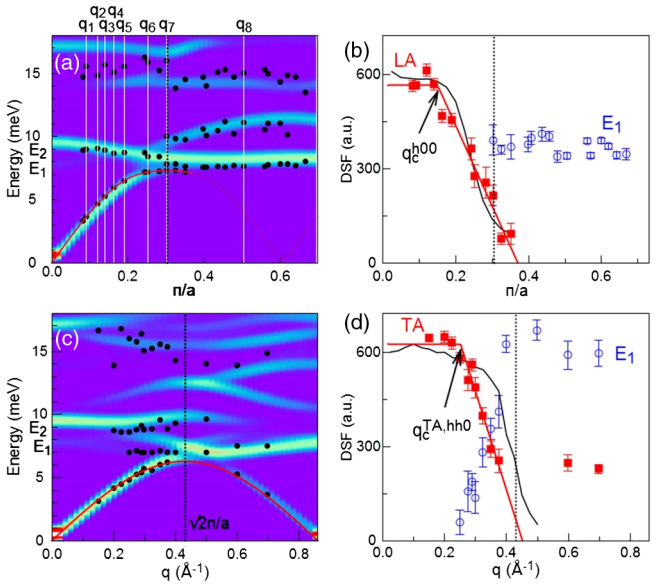

FIG. 2 (color online). Mapping of the simulated IXS intensities for (a) longitudinal phonons (LA_{001},) and (c) transverse phonons (TA^{001}_{110}). Black dots represent the fitted experimental positions. White vertical lines labeled from q_1 to q_8 in (a) indicate the cuts shown in Fig. 3. The $\mathbf{q}$ dependences of the phonon DSF of the LA_{001} and TA^{001}_{110} (filled red squares) is depicted in (b) and (d), respectively, together with the guest optical phonons at E_1 (blue circles). The solid black line stands for the DSF of the acoustic branch extracted from the simulated spectra.

the simulation and the experiment. In Fig. 3, raw data of constant $\mathbf{Q}$ scans measured along the $[0,0,6+h]$ direction (LA_{001}) are shown together with the corresponding simulated IXS spectra, convoluted with the energy profile of the instrumental resolution. For phonon wave vectors close to the Brillouin zone center all phonon spectra consist of a main peak at energies distinctly below the optical excitations, which stems from the acoustic branch and follows a linear dispersion. The very good agreement between the experimental and simulated energy profiles of the acoustic phonons confirms that their energy width, as extracted from our data, is resolution limited. The small differences can be attributed to the momentum part of the instrumental resolution that is not accounted for in the simulated scans. The intensity of the peaks, represented by the dynamical structure factor (DSF), fluctuates around a constant value for these wave vectors [Figs. 2(b) and 2(d)]. In the limit $q \to 0$, the slopes of the acoustic phonon branches correspond to the sound velocities $\nu_{\mathrm{LA}}^{[0,0,h]} = 6120$ m/s, $\nu_{\mathrm{LA}}^{[h,h,0]} = 6060$ m/s, and $\nu_{\mathrm{LA}}^{[h,h,h]} = 6040$ m/s for the longitudinal and $\nu_{\mathrm{TA}}^{(h,h,0)} = 3400$ m/s for the transverse phonon modes. From the experimentally determined sound velocities it is then possible to deduce the elastic constants $C_{11} = 135$, $C_{44} = 42$, and $C_{12} = 52$ (in GPa), which are in perfect agreement with theoretical results [18]. At energies higher than about 7 meV, the low-lying optical

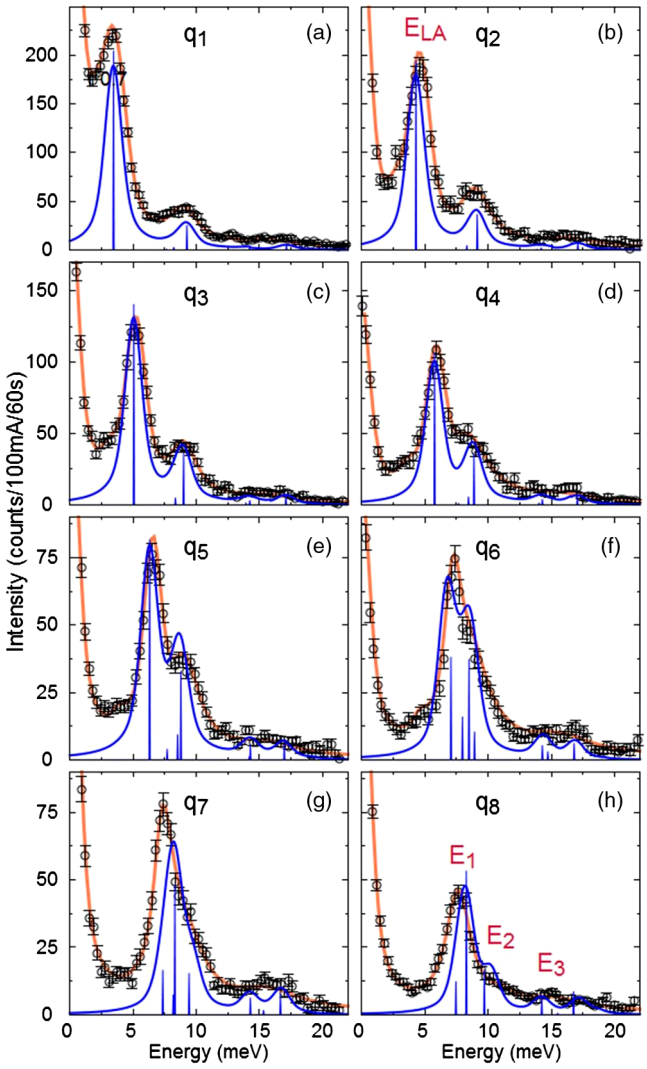

FIG. 3 (color online). (a)–(h) Constant Q scans for LA_{001}. Phonon wave vectors $\mathbf{q}_{00h}$ are labeled from q_1 to q_8 corresponding to cuts through the dispersion as depicted by the vertical white lines in Fig. 2(a). Orange lines are fits as described in the Supplemental Material [14]. Blue profiles correspond to the *ab inito* simulated IXS spectra, convoluted with the instrumental resolution. The blue vertical lines indicate the simulated phonon energies without the convolution.

phonons are described by Gaussians, centered at energies $E_1 \sim 7$–7.5 meV, $E_2 \sim 9$–10 meV, and $E_3 \sim 14$–15 meV (Fig. 3). The three excitations are interpreted as the superposition of several branches modeled by a Gaussian distribution as shown by the comparison with the calculated and unconvoluted intensities in Fig. 3 (blue vertical lines). In agreement with previous studies [16,17], the E_1 and E_2 peaks are associated with the Ba motion in the large and small cages, respectively [Fig. 1(b)], while the peak at E_3 contains optical modes involving both the host and the guest atoms. The intrinsic energy widths of the modes at E_1 (0.5 meV) and E_2 (0.6 meV) are much smaller than at E_3 (3 meV). At the zone center and for both scattering directions shown in Figs. 2(a) and 2(c), the E_1 branch cannot be resolved experimentally.

The main effect that is observed in our experimental data is an abrupt decrease of the DSF of the acoustic phonons for wave vectors higher than a critical wave vector, named $\mathbf{q}_c$, going along with an increase of the DSF of the optical phonons at E_1 [Figs. 2(b) and 2(d)]. This is accompanied by a strong bending of the dispersion relation of the acoustic excitations, with the slope approaching zero (Fig. 2). For the longitudinal polarization, the absolute values of $\mathbf{q}_c$ in the different directions of propagation are $q_c^{[0,0,h]} \sim 0.18\ \text{Å}^{-1}$ and $q_c^{[h,h,0]} \sim q_c^{[h,h,h]} \sim 0.19\ \text{Å}^{-1}$ (see Supplemental Material [14]). For the transversely polarized phonons we find $q_c^{[h,h,0]} \sim 0.25\ \text{Å}^{-1}$. No energy broadening is needed for the fitting of the acoustic and optic phonon profiles, even at wave vectors higher than $\mathbf{q}_c$. Thus, as for other materials [19], $\mathbf{q}_c$ can be interpreted as the limit of the acoustic regime since above $\mathbf{q}_c$ the acoustic character of the modes vanishes. However, this does not result in a broadening of the observed excitation, but rather in a rapid decrease of the DSF going along with an intensity transfer to the optical branch at E_1. The wave vector dependences of the simulated DSF, extracted for the LA_{001} and TA_{110}^{001} acoustic phonon branches, is plotted together with the experimental points [Figs. 2(b) and 2(d)]. The abrupt changes of the DSF are remarkably well reproduced by the DFT simulation. This confirms that the evidenced spectral weight transfer can be understood as a purely harmonic process. To get more insight into the mechanism leading to the drop of the acoustic DSF, we check whether the mean free path of the acoustic modes at $\mathbf{q}_c$ corresponds to some critical distance in the system structure. For wave vectors below $\mathbf{q}_c$, the energy width of the acoustic modes is resolution limited: it is then only possible to provide an upper bound of the intrinsic energy width, which is ~0.2 meV, corresponding to a lower limit of the lifetime of about 7 ps. Considering the local velocities at $\mathbf{q}_c$, it follows that the mean free path at $\mathbf{q}_c$ is about 16 nm for TA phonons and varies between 25 and 27 nm for LA phonons. These distances correspond to a few unit cells and cannot be directly related to any specific structural feature of clathrates. Instead, the critical wave vector $\mathbf{q}_c$ can be estimated as the $\mathbf{q}$ vector at which the crossing of the acoustic linear dispersion and the rattling mode takes place, such that $q_c^{\text{LA,TA}} \sim E_1/\nu_{\text{LA,TA}}$.

In what follows we correlate this effect of spectral weight transfer with the energy dependence of the participation ratio (PR) and the atomic participation ratio of given phonon modes as extracted from DFT calculations conducted within the harmonic approximation. The PR

$$p(\omega) = \left(\sum_{i=1}^{N} |\mathbf{u}_i(\omega_\mathbf{q})|^2\right)^2 / N \sum_{i=1}^{N} |\mathbf{u}_i(\omega_\mathbf{q})|^4 \qquad (1)$$

describes the degree of participation of the different atoms in a particular phonon mode [13]. $\mathbf{u}_i = \mathbf{e}^i(\mathbf{q})/\sqrt{M_i}$ are the atomic amplitudes with the phonon polarization vector $\mathbf{e}^i(\mathbf{q})$ and the mass M_i of atom i. In a perfect crystal, a PR close to 1 characterizes propagative phonon modes in which most of the atoms participate. On the other hand, amorphous materials usually do not achieve low-frequency PR values higher than ~0.5–0.6, which is characteristic for diffusive modes. At higher energies the PR of amorphous materials even tends to drop to ~0.2, characteristic for localized modes, meaning that a few atoms have large displacements, whereas the others are displaced only slightly or not at all [2]. Figure 4 (left) depicts a comparison between the PR of longitudinal phonons in the guest free Si_{46} framework and in the clathrate Ba_8Si_{46}. In the spectral range from 0 to 13 meV the guest-free Si_{46} framework contains acoustic modes with a PR close to 1 (~0.9–1). When filling the cages with Ba, additional nonpropagative modes with a very low PR (~0.1–0.2) are observed, causing a depression of the acoustic phonon modes in the spectral range from 7 to 13 meV. Despite their lifetime of a few picoseconds as found experimentally, these modes release their energy locally in an isotropic manner, leading to a change in the energy transport mechanism from propagative to diffusive as proposed for disordered systems [2]. This change in the character of energy propagation may be responsible for low thermal conductivity of clathrates.

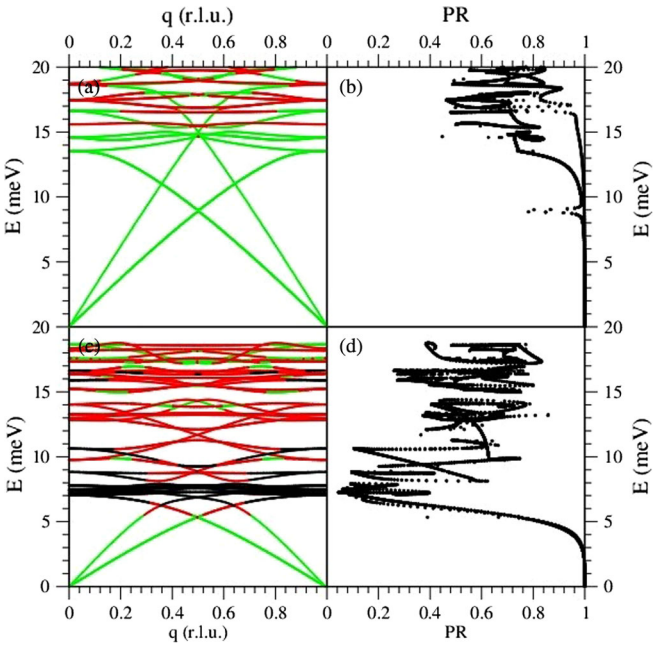

FIG. 4 (color online). Simulated dispersions (left) and participation ratios (right) for phonons propagating in the $[6+h,0,0]$ direction in Si_{46} [top panels (a),(b)] and Ba_8Si_{46} [bottom panels (c),(d)]. Modes in (a),(c) are color coded with respect to their PR. Green means a high PR; red and black correspond to intermediate and low PR, respectively.

The particularity of this localization of long-wavelength phonons is that it occurs between the guest and host phonon subsystems of the clathrate, which are intrinsically entangled. To further investigate this localization phenomenon we introduce the atomic participation ratio (APR)

$$p_i(\omega) = |\mathbf{u}^i(\omega_\mathbf{q})|^2 / \left(N \sum_{i=1}^{N} |\mathbf{u}_i(\omega_\mathbf{q})|^4 \right)^{1/2} \quad (2)$$

with $p(\omega) = (\sum_{i=1}^{N} p_i(\omega))^2$, which disentangles the contributions of Ba and Si atoms on the respective Wyckoff sites to the lattice dynamics at a given energy. In Fig. 5(a) the APR of the different Wyckoff sites is shown as a function of energy for a powder average of phonon modes (i.e., a random distribution of $\mathbf{q}$ vectors within the first BZ). Between 0 and 6 meV, the phonon spectrum is essentially composed of either LA or TA phonon branches as can be inferred from Fig. 4. Below 2 meV the APR is constant with almost the same motions of Ba and Si atoms, which is characteristic for acoustic waves close to the Brillouin zone

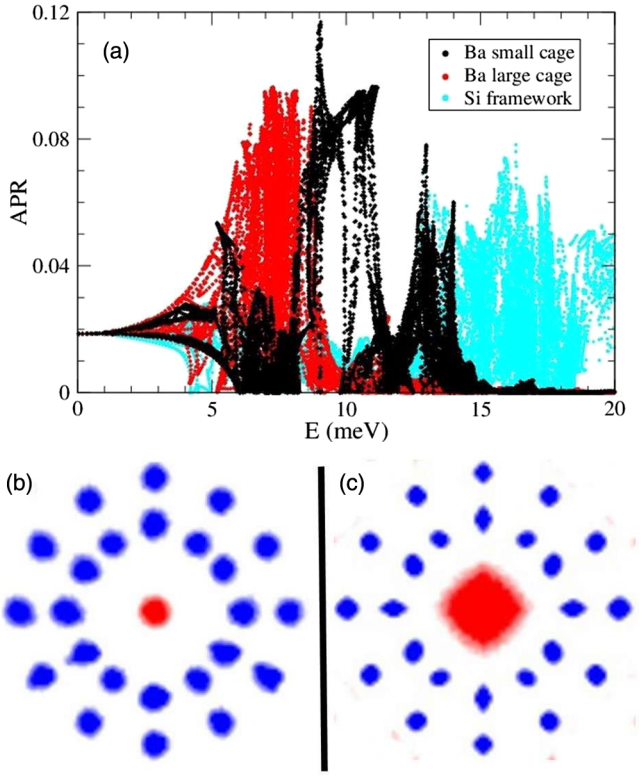

FIG. 5 (color online). (a) Atomic participation ratio, as defined in Eq. (2), obtained for a powder average of phonon modes in Ba_8Si_{46}, with each color representing a given Wyckoff site. (b), (c) show the projection of the average atom distribution of atoms in the large $BaSi_{24}$ cluster resulting from phonon motions in different frequency intervals as determined for the powder average of modes whose APR is depicted in (a). (b) Corresponds to modes with acoustic character in the range 0–2 meV; (c) Depicts modes in the range from 6 to 8 meV.

center. For energies between 2 and 6 meV, the acoustic phonons involve increasing motion of Ba atoms in the large $BaSi_{24}$ cages, whereas the participation of the Si atoms decreases, as also observed in the partial vibrational density of states calculated in Ref. [16]. In the energy range between 6 and 9 meV, the acoustic branches are completely localized and the optical phonons consist essentially of displacements of Ba atoms in the large cages, as also visible in the partial density of states [16]. The optical phonons in the energy range between 9 and 11 meV arise from displacements of Ba atoms in the small $BaSi_{20}$ cages, whereas those at higher energies correspond to motions dominated by Si atoms. In Figs. 5(b) and 5(c) the characteristic displacement pattern of phonon modes for two different energy intervals is shown for the large $BaSi_{24}$ cages. For the energy interval from 0 to 2 meV [Fig. 5(b)] the modes have acoustic character and therefore show a similar displacement pattern for all atoms. For modes in the energy range from 6 to 8 meV [Fig. 5(c)], the Ba atoms in the large cages show much larger displacements, corresponding to a strongly enhanced APR.

In summary, our combined experimental and computational study of the lattice dynamics in Ba_8Si_{46} demonstrates that the main effect of the guest-host interaction is a spectral weight transfer between acoustic and guest-dominated optical phonons. This spectral weight transfer goes along with a strong bending of the acoustic dispersion starting at a critical wave vector $\mathbf{q}_c$, which can be interpreted as the limit of the acoustic regime. Surprisingly, the guest-host interaction and its consequences can be understood as a purely harmonic process; i.e., it is not dominated by phonon scattering processes. The acoustic phonons keep a very long lifetime as well as their propagative nature, until $\mathbf{q}_c$ is reached: at this point the character of the acoustic phonons changes, resulting in modes with an increasing contribution of the guest atoms and a very low participation ratio. This localization of the propagative phonons leads to a transition from propagative to diffusive-like energy transport.

S. Pailhès acknowledges support from the CNRS Interdisciplinary Programs Fund (AAP INSIS 2012) and from the French National Research Agency (ANR-13-PRGE-0004), and S. Paschen acknowledges support from the Austrian Science Fund (TRP 176-N22). This work has been carried out within the European C-MAC network.

*To whom correspondence should be addressed.
stephane.pailhes@univ-lyon1.fr

[1] M. De Boissieu, S. Francoual, M. Mihalkovic, K. Shibata, A. Q. R. Baron, Y. Sidis, T. Ishimasa, D. Wu, T. Lograsso, L.-P. Regnault, F. Gahler, S. Tsutsui, B. Hennion, P. Bastie, T. J. Sato, H. Takakura, R. Currat, and A. P. Tsai, Nat. Mater. **6**, 977 (2007).
[2] Y. M. Beltukov, V. I. Kozub, and D. A. Parshin, Phys. Rev. B **87**,134203 (2013).
[3] A. Bodapati, P. K. Schelling, S. R. Phillpot, and P. Keblinski, Phys. Rev. B **74**,245207 (2006).
[4] L. Chaput, Phys. Rev. Lett. **110**, 265506 (2013).
[5] E. S. Toberer, A. Zevalkink, and G. Jeffrey Snyder, J. Mater. Chem. **21**, 15843 (2011).
[6] Toshiro Takabatake, Koichiro Suekuni, Tsuneyoshi Nakayama, and Eiji Kaneshita, Rev. Mod. Phys. **86**, 669 (2014).
[7] A. San Miguel and P. Toulemonde, High Press. Res. **25**, 159 (2005).
[8] M. Marek Koza, M. R. Johnson, R. Viennois, H. Mutka, L. Girard, and D. Ravot, Nat. Mater. **7**, 805 (2008).
[9] H. Euchner, S. Pailhès, L. T. K. Nguyen, W. Assmus, F. Ritter, A. Haghighirad, Y. Grin, S. Paschen, and M. de Boissieu, Phys. Rev. B **86**, 224303 (2012).
[10] J. Baumert, C. Gutt, V. P. Shpakov, J. S. Tse, M. Krisch, M. Muller, H. Requardt, D. D. Klug, S. Janssen, and W. Press, Phys. Rev. B **68**, 174301 (2003).
[11] N. J. English, J. S. Tse, and D. J. Carey, Phys. Rev. B **80**, 134306 (2009).
[12] C. H. Lee, I. Hase, H. Sugawara, H. Yoshizawa, and H. Sato, J. Phys. Soc. Jpn. **75**, 123602 (2006).
[13] J. Hafner and M. Krajci, J. Phys. Condens. Matter **5**, 2489 (1993).
[14] See Supplemental Material at http://link.aps.org/supplemental/10.1103/PhysRevLett.113.025506 for details of the high pressure synthesis, structural and thermal characterizations. IXS data of LA phonons propagating along [111] and [110] directions are shown. A depth analysis of the IXS resolution function for crystals, using also data on pure Silicon, is provided. Details on the DFT calculations presented in the main text are included.
[15] A small longitudinal component, $\mathbf{q}_l = 0.1$, is required to avoid a large contamination from the Bragg peak. The data were measured at wave vectors $\mathbf{Q} = \mathbf{G}_{006} + \mathbf{q}_{h,h,0.1}$
[16] J. I Castro and A. Lopez, Phys. Rev. B **72**, 224507 (2005).
[17] R. Lortz, R. Viennois, A. Petrovic, Y. Wang, P. Toulemonde, C. Meingast, M. M. Koza, H. Mutka, A. Bossak, and A. San Miguel, Phys. Rev. B **77**, 224507 (2008).
[18] D. Connétable, Phys. Rev. B **82**, 075209 (2010).
[19] M. de Boissieu, R. Currat, S. Francoual, and E. Kats, Phys. Rev. B **69**, 054205 (2004).